New Journal of Physics
The open access journal at the forefront of physics

Deutsche Physikalische Gesellschaft DPG
IOP Institute of Physics

Published in partnership with: Deutsche Physikalische Gesellschaft and the Institute of Physics

OPEN ACCESS

RECEIVED
8 June 2015

REVISED
6 August 2015

ACCEPTED FOR PUBLICATION
17 August 2015

PUBLISHED
16 September 2015

PAPER

A phase-space approach for propagating field–field correlation functions

Gabriele Gradoni[1], **Stephen C Creagh**[1], **Gregor Tanner**[1], **Christopher Smartt**[2] **and David W P Thomas**[2]

[1] School of Mathematical Sciences, University of Nottingham, University Park, NG7 2RD, UK
[2] George Green Institute for Electromagnetics Research, University of Nottingham, University Park, NG7 2RD, UK

E-mail: gregor.tanner@nottingham.ac.uk

Keywords: electromagnetic radiation, wave propagation, Wigner functions, semiclassical theories and applications, wave fronts and ray tracing

Abstract

We show that radiation from complex and inherently random but correlated wave sources can be modelled efficiently by using an approach based on the Wigner distribution function. Our method exploits the connection between correlation functions and the Wigner function and admits in its simplest approximation a direct representation in terms of the evolution of ray densities in phase space. We show that next leading order corrections to the ray-tracing approximation lead to Airy-function type phase space propagators. By exploiting the exact Wigner function propagator, inherently wave-like effects such as evanescent decay or radiation from more heterogeneous sources as well as diffraction and reflection can be included and analysed. We discuss in particular the role of evanescent waves in the near-field of non-paraxial sources and give explicit expressions for the growth rate of the correlation length as a function of the distance from the source. The approximations are validated using full-wave simulations of model sources. In particular, results for the reflection of partially coherent sources from flat mirrors are given where the influence of Airy function corrections can be demonstrated. We focus here on electromagnetic sources at microwave frequencies and modelling efforts in the context of electromagnetic compatibility.

1. Introduction

Predicting the properties of wave fields in complex environments is an extremely challenging task of crucial importance to a wide variety of technological and engineering applications, such as vibroacoustics [1] or electromagnetic (EM) wave modelling [2]. In particular, characterizing the radiation of EM sources reliably, both in free space and within enclosures, is a longstanding research issue [3, 4]. In the context of electromagnetic compatibility (EMC), digital circuits and large printed circuit boards (PCB) embed thousands of electronic devices and metallic tracks and can produce fields reaching dangerous but hard-to-predict levels [5].

In this paper, we set out an approach for propagating such complex and statistically characterized wave fields exploiting Wigner distribution function (WDF) techniques. This approach has its origin in quantum mechanics [6], but has more recently found widespread attention in optics, see [7–9] for an overview. The WDF formalism offers a direct route to pure ray-tracing approximations in an operator implementation [1], while still capturing in its exact formulation the full wave dynamics. The formalism allows one to efficiently treat radiation from complex sources, often having a statistical character. Complexity arises here through the stochastic nature of the radiated field which may be best described by considering time or frequency averages and thus looking at an ensemble of system realizations. A statistical representation is then appropriate and computationally more efficient than a purely deterministic treatment.

The method introduced below exploits a connection between the field–field *correlation function* (CF) and the WDF [10–12]. Both quantities have been studied intensively in the physics and optics literature. For wave chaotic systems, Berry's conjecture postulates a universal CF equivalent to correlations in Gaussian random fields [13, 14]. Non-universal corrections can be retrieved by linking the CF to the Green function of the system

[15–18]. In this paper, we describe how field-field CFs can be efficiently propagated using ideas based on ray propagation in phase-space. We discuss furthermore non-paraxial effects as well as including near field effects due to evanescent wave contributions. A systematic expansion of the Wigner function propagator including next-to-leading-order effects in the propagating regime leads to Airy-function integral kernels containing the ray-tracing propagator in the small wavelength limit, akin to the treatments in [10, 19]. We show that the Airy propagator improves the reconstruction of the WF when higher order effects become important such as in the presence of destructive interference in configuration space. We also show that our WDF representation confirms the validity of the generalized form of the Van Cittert-Zernike (VCZT) theorem discussed in [20]. We give a natural extension of this generalized VCZT for non-paraxial sources and in the near-field region where evanescent waves play a prominent role.

We illustrate these techniques in the context of applications in EMC and related issues. Here, the system under investigation represents a high-density interconnect of integrated electronic circuits. Simulating EM field distributions in a reliable way is highly topical; in addition, the wave CF can be measured explicitly in this regime [21], thus providing the necessary input information for numerical simulations. The system under consideration in this paper consists of a series of parallel tracks carrying partially correlated currents, and mimics the typically very complex EM sources found on PCBs. The method has much wider application, however. In particular, when combined with fast phase-space propagation methods such as the *discrete flow mapping* techniques developed in the context of vibro-acoustics [1, 22], the proposed WDF approach offers an ideal platform for developing a universal high-frequency simulation method.

2. Phase-space representation of classical fields

Radiation from simple EM sources such as antennae can be characterized deterministically through classical electrodynamical methods [23]. Even though such sources are regular and homogeneous, efficiently predicting far-field emission from the near-field pattern requires non-trivial effort if the sources are extended over many wavelengths [24]. EM sources are becoming increasingly complex, however, and the problem of radiation from digital circuits or PCBs presents even greater challenges. Modelling such sources deterministically is often infeasible due to the complexity of the structures, whose details may not even be known in practice. Each component of such a complex EM source is typically driven by unknown sets of random voltages, subject to fast transients [25]. This is due to the presence of a multitude of electronic components whose switching behaviour depends on the instantaneous operation mode of the circuit, and whose excitation signals are intrinsically random, or highly sensitive to frequency [21]. Consequently, the physical investigation of these scenarios challenges existing analytical and numerical techniques, and calls for more sophisticated modelling tools.

It is thus natural to use statistics as a language for describing the radiation from such complex sources. Specifically, we do not attempt to characterize or propagate the field itself, which is typically hard to obtain in practice, but rather its two-point CF. It has been demonstrated in [21] that corresponding measurements are feasible in the context of emission from electronic devices and PCBs. Here we describe the basic elements needed to use such measurements as input for a practical algorithm with which to predict field intensities and correlations away from the source. Initially we consider radiation into free space in section 4 by studying a simple model source and a more realistic source obtained from a full field simulation. In section 5, we describe an application to a problem with reflecting boundaries, which is a first step towards our ultimate goal of extending the method to propagation of CFs in more complex environments such as cavities and larger structures.

We start from a planar source at $z = 0$, parametrized by coordinates $x = (x_1, \ldots x_d)$ with $d = 1$ or 2 in general, and radiating into the half-space $z > 0$. We aim to predict the CF

$$\Gamma_z\left(x_B, x_A\right) = \left\langle \psi\left(x_B, z\right)\psi^*\left(x_A, z\right)\right\rangle \tag{1}$$

for $z > 0$ under the assumption that it can be measured (or otherwise modelled) near the source screen $z = 0$, over different source field configurations. Here, $\langle . \rangle$ denotes an ensemble average over different source field correlations such as a time or frequency-band average. Furthermore, $\psi(x, z)$ denotes one of the tangential field components in the frequency domain. The results easily extend to cross-correlation between different components.

In the past, the focus has often been on predicting the propagation of probability density functions of waves passing through time-domain random [26] or turbulent [27] media. In our approach, the propagation itself is treated deterministically, whereas the radiation from the source is characterized statistically. This can be done, for example, by measuring the spatial field along a surface close to the source and determining the source CF by averaging the signal over time. We thereby eliminate statistical fluctuations carried by the wave fields by ensemble averaging physical observables over suitable parameters.

We now present the CF propagation rule explicitly for single field components. Polarization effects can also be accounted for by propagating the field–field correlation tensor, which can be derived from the dyadic free-space Green's function [28, 29].

The field in the region $z > 0$ is naturally presented in terms of the partial Fourier transform,

$$\phi(p, z) = \int \mathrm{e}^{-\mathrm{i}kp\cdot x}\psi(x, z)\,\mathrm{d}x,$$

where $\psi(x, z)$ denotes a field component on the screen itself ($z = 0$) or above ($z > 0$) and $k = \sqrt{k_x^2 + k_z^2}$ is the wave number. The radiated fields can then be reconstructed using the evolution of this partial field. This can be calculated by using the dyadic second Green identity which, in a source-free region, becomes the dyadic version of Huygen's principle [30]. Being a convolution integral, the partial Fourier transform of the surface integral transforms to an algebraic equation. Then, the boundary conditions given by the fields sampled in the near-field region of the source can be used to eliminate the magnetic field in such an equation. The result of this procedure, restricted to the electric field components parallel to the source plane, is the following inhomogeneous plane-wave solution

$$\phi(p, z) = \mathrm{e}^{\mathrm{i}kzT(p)}\phi(p, 0), \tag{2}$$

where

$$T(p) = \begin{cases} \sqrt{1 - |p|^2} & \text{if } |p|^2 \leqslant 1 \\ \mathrm{i}\sqrt{|p|^2 - 1} & \text{if } |p|^2 > 1. \end{cases} \tag{3}$$

For the moment, we neglect waves incident from the right and thus only describe radiation from a strong, directional source; including incoming waves at the interface can be introduced formally using the boundary integral equations according to the discussion in [31]. An example of this scenario, involving a planar reflector beyond the source, will be given in section 5. Here, $p = (p_1, \ldots, p_d)$ takes the meaning of a momentum tangential to the d-dimensional source plane. In the ray-dynamical limit, we may identify

$$|p| = \sin\alpha, \tag{4}$$

$$T(p) \equiv p_z = \cos\alpha, \tag{5}$$

where the angle α describes the direction of the ray with respect to the local outward normal to the source. In this perspective, $T(p)$ represents a generalized kinetic energy of the ray. The case $|p|^2 > 1$ in (3) corresponds to evanescent propagation, which does not contribute to the far-field, but may be detectable in the near field; see also the discussion in sections 4.2 and 4.3. In order to represent wave fields in phase-space using canonical coordinates (x, p) parallel to the source plane, we define the WDF

$$W_z(x, p) = \int \mathrm{e}^{-\mathrm{i}kp\cdot s}\Gamma_z(x + s/2, x - s/2)\,\mathrm{d}s \tag{6}$$

$$= \left(\frac{k}{2\pi}\right)^d \int \mathrm{e}^{\mathrm{i}kx\cdot q}\left\langle \phi(p + q/2, z)\phi^*(p - q/2, z)\right\rangle \mathrm{d}q. \tag{7}$$

Upon insertion of (2) in (6), and by exploiting the inverse transformation to represent the source correlation (at $z = 0$) in terms of the source Wigner function $W_0(x, p)$, we find

$$W_z(x, p) = \int \mathcal{G}_z(x, p, x', p')\, W_0(x', p')\,\mathrm{d}x'\mathrm{d}p'. \tag{8}$$

This provides us with a propagator of the Wigner function taking the form

$$\mathcal{G}_z(x, p, x', p') = \left(\frac{k}{2\pi}\right)^d \delta(p - p') \int \mathrm{e}^{\mathrm{i}k(x-x')\cdot q + \mathrm{i}kz(T(p+q/2) - T^*(p-q/2))}\,\mathrm{d}q,$$

where the δ-function represents translational invariance in x and the corresponding conservation of momentum. Equation (2) provides a scheme to propagate wave densities in phase-space for arbitrary sources, no matter how complex or rapidly varying. The propagation of the CFs themselves can subsequently be retrieved by an inverse Fourier transform of (8). That is,

$$\Gamma_z\left(x_B, x_A\right) = \left(\frac{k}{2\pi}\right)^d \int \mathrm{e}^{\mathrm{i}ks\cdot p}\, W_z(x, p)\,\mathrm{d}p, \tag{9}$$

where $x = (x_A + x_B)/2$, and $s = x_B - x_A$. The intensity I_z as function of the distance z can be retrieved using [8]

$$I_z(x) = \Gamma_z(x, x) = \left(\frac{k}{2\pi}\right)^d \int W_z(x, p)\,\mathrm{d}p. \tag{10}$$

3. Ray tracing approximations

Asymptotic approximation of the propagator (9) leads to a direct propagation method for the WDF in terms of rays [9, 10, 32–34]. We will give a derivation of this ray limit below and will also discuss more subtle wave effects such as evanescent decay into the near-field and higher order (in $1/k$) wave corrections.

The simplest ray-based approximation is obtained under the assumption that the CF is quasi-homogeneous at the source, that is, $\Gamma_0(x_B, x_A) = \Gamma_0(x + s/2, x - s/2)$ varies only slowly with respect to x on the scale of a wavelength; this is also referred to as a Collet–Wolf source [35]. In that case, significant contributions to (9) are obtained only for small q and we can expand the phase difference $\Delta T(p, q) = T(p + q/2) - T^*(p - q/2)$ around $q = 0$.

In the region $|p|^2 \leqslant 1$ corresponding to propagating waves, the difference ΔT receives contributions only from odd powers of q. Neglecting cubic and higher order terms we find that

$$\mathcal{G}_z(x, x'; p, p') \approx \delta\left(x - x' - \frac{zp}{T(p)}\right)\delta(p - p'). \tag{11}$$

This is the Frobenius–Perron (FP) propagator [36] for radiation into free space and leads to the evolution [10]

$$W_z(x, p) \approx W_0\left(x - \frac{zp}{T(p)}, p\right) \tag{12}$$

of the WDF in the region $|p|^2 \leqslant 1$. This approximation is equivalent to identifying the propagation of the WDF with the propagation of phase space densities along rays according to the evolution

$$\begin{aligned} x &= x' + \frac{zp}{T(p)} \\ p &= p'. \end{aligned} \tag{13}$$

The paraxial approximation is obtained by using the linearized flow in the regime $|p|^2 \ll 1$ [9]. Outside this regime, the full flow has asymptotes along $|p|^2 = 1$, the transition to evanescent propagation. Note that inserting equation (12) in equation (9) and including only the contributions from the propagating region $|p|^2 \leqslant 1$ leads to

$$\Gamma_z\left(x_B, x_A\right) \approx \left(\frac{k}{2\pi}\right)^d \int \mathrm{e}^{\mathrm{i}kps} W_0\left(x - \frac{zp}{T(p)}, p\right)\mathrm{d}p. \tag{14}$$

In the paraxial regime, that is for $|p|^2 \ll 1$, and for quasi-homogeneous sources, equation (14) retrieves the well-known van Cittert-Zernike theorem (VCZT) or generalization thereof [11, 20, 37]. In the next section we will show how to extend the VCZT to the non-paraxial regime and including evanescent waves.

Expanding ΔT to higher orders in q leads to a propagator which is capable of mapping less homogeneous CF's. Including cubic terms leads in the 2D case, for example, to the Airy form

$$\mathcal{G}_z(x, p, x', p') \approx \delta_a\left(x - x' - \frac{zp}{T(p)}\right)\delta(p - p'), \tag{15}$$

where

$$\delta_a(u) = a\mathrm{Ai}(au),$$

with $a = 2k/(kzT'''(p))^{1/3}$ and Ai denotes the Airy function. Note that $\lim_{|a|\to\infty}\delta_a(u) = \delta(u)$, so the FP form is obtained in the limit of large wavenumber k as expected. Similar results have been obtained in the context of the propagation of EM waves through inhomogeneous media [19].

Further improvements over the basic FP propagation (11) are obtained by accounting for evanescent decay into the near-field, which emerges from contributions $|p|^2 > 1$ in equation (8). Since the kinetic operators in equation (9) now add constructively, the leading contribution is formed by the zeroth order term in the expansion of $\Delta T(p, q)$ and we obtain

$$W_z(x, p) \approx \mathrm{e}^{-2kz\sqrt{|p|^2-1}} W_0(x, p), \qquad |p|^2 > 1. \tag{16}$$

Improved approximations may be achieved by treating the exponent beyond leading order, but we find that (16) gives a good description of evanescent decay already as discussed in the next section.

4. Radiation into free space

We now test the effectiveness of the FP propagator in the simple case of radiation into free space. The first example treated in section 4.1 assumes a quasi-homogenuous source distributed according to the Gaussian Schell model [38]. We will examine the near-field behaviour in more detail in section 4.2, considering in

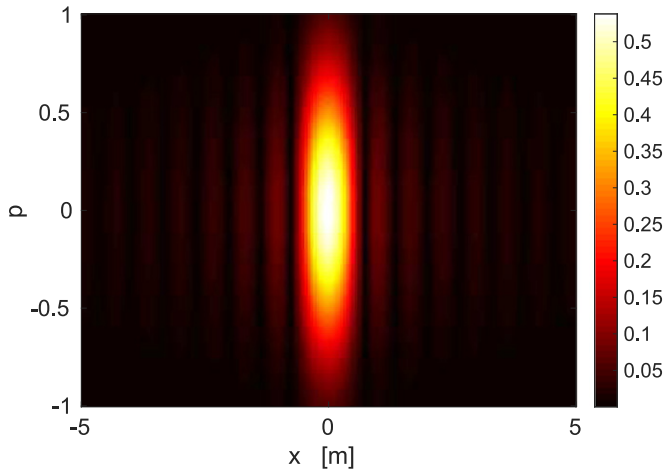

Figure 1. Absolute value of the WDF of a 1D Gaussian Schell correlation function at $z = 0$ m. The radiation frequency is $f = 1$ GHz corresponding to $\lambda = 0.3$ m. The distribution widths are $\sigma_x = 1.0$ m, and $\sigma_s = 0.1$ m.

particular the limit of completely uncorrelated sources. In a second example in section 4.3, we consider a more complex set-up mimicking the more realistic sources expected in typical EM applications. We will restrict ourselves in these examples to 2D models (so $d = 1$) and characterize the behaviour of field–field correlations by focusing on the propagation of *one* field component along z. We select the field tangent to the source.

4.1. Propagation of Gaussian Schell model

Using a simple 2D model for the emission of partially coherent EM radiation, we assume a source correlation in terms of a truncated 1D Gaussian Schell model [38]

$$\Gamma_0\left(x_B, x_A\right) = I_0 \exp\left[-\frac{\left(x_B - x_A\right)^2}{2\sigma_s^2}\right] \exp\left[-\frac{\left(x_B + x_A\right)^2}{8\sigma_x^2}\right] \times \chi_l\left(x_B\right) \chi_l\left(x_A\right), \tag{17}$$

where l is the length of the source. Here, the characteristic functions

$$\chi_l(x) = \begin{cases} 1, & |x| \leqslant \frac{l}{2}, \\ 0, & |x| \geqslant \frac{l}{2} \end{cases} \tag{18}$$

account for the finite size of the source. The quasi-homogeneity condition can be expressed through demanding $\sigma_s \sim \lambda \ll \sigma_x$, where $\lambda = 2\pi/k$ is the optical wavelength. The source WDF is then found to be

$$W_0(x, p) = I_0 \exp\left[-\frac{x^2}{2\sigma_x^2}\right] \sqrt{\frac{\pi}{2}}\, \sigma_s \exp\left(-\frac{k^2 p^2 \sigma_s^2}{2}\right) \times \left[\operatorname{erf}\left(\frac{l - 2\,|x|}{\sigma_s \sqrt{2}} - \mathrm{i}\frac{kp\sigma_s}{\sqrt{2}}\right) - \operatorname{erf}\left(-\frac{l - 2\,|x|}{\sigma_s \sqrt{2}} - \mathrm{i}\frac{kp\sigma_s}{\sqrt{2}}\right)\right]. \tag{19}$$

For extended sources, for which $l \gg \lambda$, and for x inside the region occupied by the source, equation (19) simplifies to

$$W_0(x, p) \approx \sqrt{2\pi}\, \sigma_s I_0 \exp\left[-\frac{x^2}{2\sigma_x^2} - \frac{k^2 p^2 \sigma_s^2}{2}\right]. \tag{20}$$

Figure 1 shows the WDF in phase-space at $z = 0$ for a spatially extended source [39]. Here, and in all other computations with the Gaussian Schell model, we work at a frequency of operation of 1 GHz corresponding to $\lambda = 0.3$m and choose $\sigma_x = 1.0$ m, $\sigma_s = 0.1$ m.

Figure 2 shows the propagation of (19) as computed through the full integral operator (8) together with the propagation obtained by the FP approximation (12). There is surprisingly good agreement between the exact and approximate behaviour even far from the paraxial regime. This is remarkable given that the ray tracing approximation is only valid to leading order. This constitutes a major computational advantage as the FP

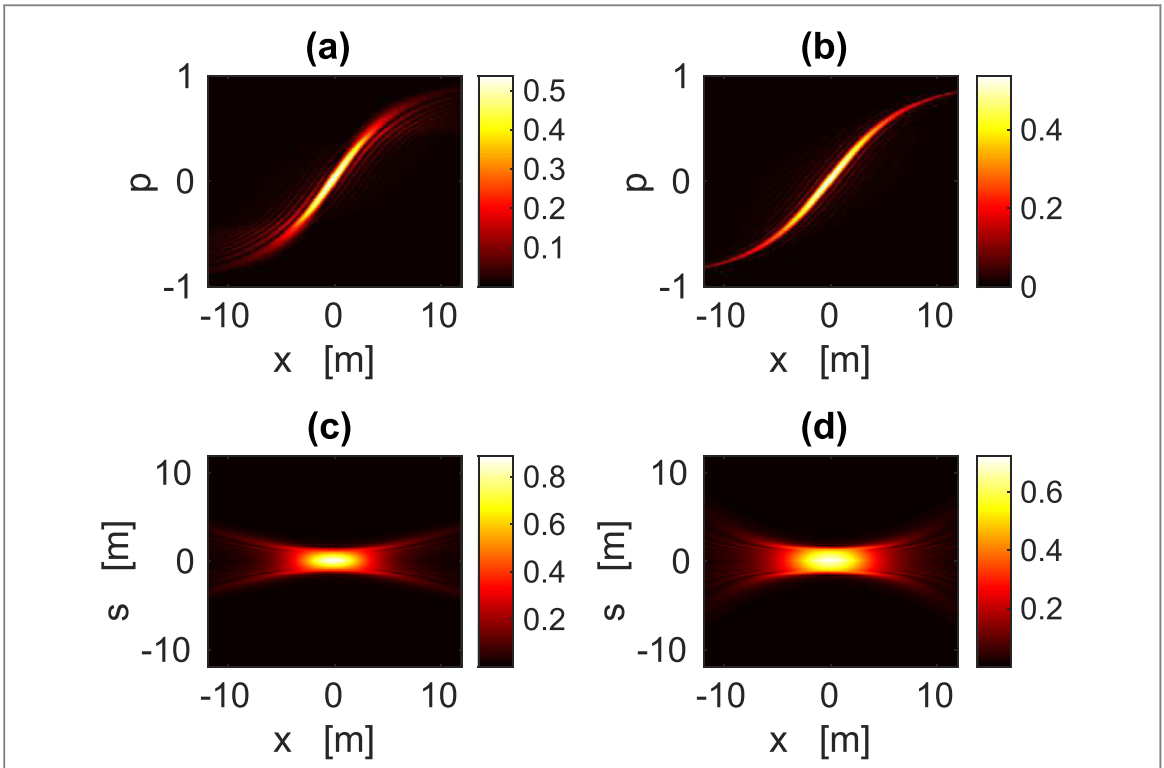

Figure 2. Propagated Wigner distribution function (a), (b) and correlation function (c), (d) of a partially-coherent (1D Gaussian Schell) near-homogeneous source: exact ((a) and (c)) versus approximate—Frobenius–Perron—((b) and (d)) computation at $z = 10\lambda$ (all in absolute values). The radiation frequency is $f = 1$ GHz. The distribution widths are $\sigma_x = 1$ m, and $\sigma_s = 0.1$ m.

approximation reduces an integral equation to a coordinate transformation. The overall behaviour shown in figures 2(a) and 2(b) reflects the distribution shearing due to the geometrical ray propagation based on equation (13); see also [9]. The CFs can now be obtained by a back transformation according to equation (9) and are shown in figures 2(c) and (d).

4.2. Non-paraxial VCZT

In the following, we will focus on near-field effects for small distances from the source as a function of the source correlation parameter σ_s. We are in particular interested in how the correlation length propagates in the near-field before reaching the linear VCZT regime.

In the near-field limit, the WDF shows exponentially decaying evanescent components according to (16), while the WDF remains essentially unchanged for the propagating part $|p|^2 \leqslant 1$. This leads to a model for the WDF with source distribution (20) of the form

$$W_z(x, p) \approx \sqrt{2\pi}\,\sigma_s I_0 \exp\left[-\frac{x^2}{2\sigma_x^2} - \frac{k^2 p^2 \sigma_s^2}{2}\right] \times \begin{cases} 1 & \text{if } |p|^2 \leqslant 1 \\ \mathrm{e}^{-2kz\sqrt{|p|^2-1}} & \text{if } |p|^2 > 1. \end{cases} \tag{21}$$

Far enough from the source, such that evanescent components have completely decayed, while close enough that evolution in the propagating region of phase space can still be neglected, we model the WDF using

$$W_z(x, p) \approx \sqrt{2\pi}\,\sigma_s I_0 \exp\left[-\frac{x^2}{2\sigma_x^2} - \frac{k^2 p^2 \sigma_s^2}{2}\right] \times \begin{cases} 1 & \text{if } |p|^2 \leqslant 1 \\ 0 & \text{if } |p|^2 > 1. \end{cases} \tag{22}$$

Using the inverse Fourier transform, equation (9), we now obtain the CF from the WDF given by equation (21) or equation (22). In figure 3 we show the resulting near-field evolution of the CF, placing the midpoint $x = (x_A + x_B)/2 = 0$ at the centre of the source.

One observes that in the presence of evanescent waves, that is for small kz, the CF decays rapidly to zero not showing the typical sinc function oscillations. The correlation width increases as one moves away from the source until the sinc function form is established whose width then increases linearly according to the VCZT. In particular, in the near-field regime, the width Δs of the CF is smaller than the wavelength λ, but it increases

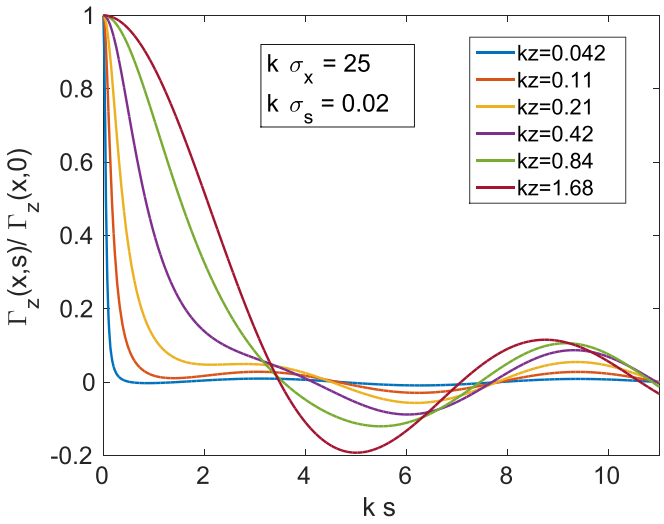

Figure 3. Evolution of the correlation function along the line $x = 0$ for a selected (partially) correlated source, from $kz = 0.42$ (blue solid line) to $kz = 1.68$ (brown solid line). The physical dimension of the source ($k\sigma_x = 25$) and its correlation length ($k\sigma_x = 0.02$) are the same for all the curves.

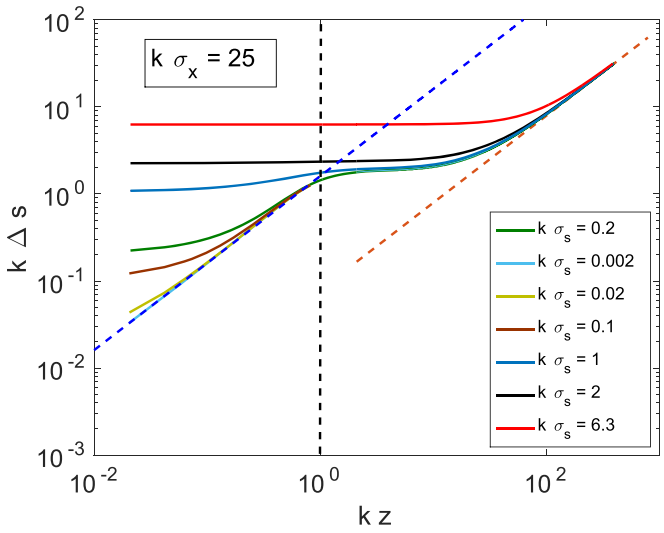

Figure 4. Evolution of the correlation length Δs with z on a log-log scale at $x = 0$ and for a partially correlated 1D source. Evanescent waves drive the increase of the correlation length (blue dashed line) described by a universal linear regime in equation (25) for sources with sub-wavelenght correlations. A plateau is observed between $kz \approx 1$ and the so-called *Rayleigh* range as defined in [20, 40]. For large kz the canonical VCZT regime sets in (red dashed line), for which the correlation length increases according to equation (28).

towards λ as z approaches and exceeds λ. The second moment of the CF is not defined in the near field regime and cannot therefore be used to define a correlation length. Instead, we define the correlation lengths to be the spacing at which the correlation has fallen by a factor $1/\sqrt{e}$:

$$\Gamma_z(x + \Delta s/2,\, x + \Delta s/2)/\Gamma_z(x,\, x) = e^{-1/2}. \tag{23}$$

Note that for a Gaussian CF such as assumed for the source in (17), this definition coincides with the standard variance: $\Delta s = \sigma_s$.

We can now obtain the correlation lengths from exact wave propagation calculations. The results are shown in figure 4 as a function of the distance z for different source correlation lengths σ_s.

From equations (21) and (22), one can estimate the growth rate both in the near and the far field. Including non-paraxial effects, there are three different regimes:

(i) in the deep near field, with $kz < 1$ and $k\sigma_s < 1$, the correlation length increases linearly with a slope that is independent of the frequency as well as of σ_s and σ_x (blue dashed line in figure 4);

(ii) a no-growth regime with $\Delta s = \text{const.}$

– For $k\sigma_s < 1$, one finds $k\Delta s \approx 1$ in the range $1 < kz < k\sigma_x$;

– For $k\sigma_s > 1$, then $\Delta s = \sigma_s$ in the range $0 < kz < (k\sigma_s)(k\sigma_x) = kz_c$.The latter regime has already been described for paraxial sources in [20, 40] where the onset of the VCZT regime was described as the Rayleigh range $z_c = k\sigma_s\sigma_x$ in our notation;

(iii) the VCZT regime for large z, or $z > z_c$ for $k\sigma_s > 1$, with a linear growth of the correlation length according to

$$\Delta s \propto \frac{\lambda}{l} z, \tag{24}$$

with a slope depending on the ratio of wavelength to source dimension l (red dashed line in figure 4).

We now motivate these three regimes in more detail, beginning with case (i), which corresponds to $k\sigma_s < 1$, $kz < 1$. The WDF described by (21) then decays slowly along the p axis as $|p|$ increases beyond the propagating region $|p|^2 = 1$. In the extreme nearfield the CF is proportional to the inverse Fourier transform of the function

$$W_z(x, p) \sim \mathrm{e}^{-2kz|p|}$$

of p, that is,

$$\Gamma_z(s) \sim \frac{2kz/\pi}{(2kz)^2 + (ks)^2}.$$

The correlation length defined by equation (23) then takes the form

$$\Delta s \approx 2\sqrt{\sqrt{\mathrm{e}} - 1}\; z \approx 1.6109\, z. \tag{25}$$

That is, we find in regime (i) that evanescent decay of the sub-wavelength correlations in the source dominates in such a way that there is a *universal* growth rate in the correlation length. The numerical value of the slope in (25) is particular to the form taken in equation (23) for the correlation length, but the qualitative conclusion applies more generally. The presence of evanescent waves thus leads to an increase of the correlation length in the near field in this regime which is typically faster than in the VCZT regime. This is important for sources that show fluctuations on scales smaller than the wavelength, such as in the case of a fully uncorrelated source $\sigma_s = 0$, which may serve as a model for thermal sources [41].

The plateau behaviour corresponding to regime (ii) arises when z is sufficiently large that (22) describes the WDF, while $k\sigma_s < 1$. The CF is then proportional to the inverse Fourier transform

$$\Gamma_z(s) \sim \frac{1}{\pi}\mathrm{sinc}(ks)$$

of the function

$$W_z(x, p) \sim \begin{cases} 1, & |p|^2 \leqslant 1, \\ 0, & |p|^2 > 1 \end{cases} \tag{26}$$

of p. In this case the correlation length defined by equation (23) takes the form

$$k\Delta s \approx 1.6443 \tag{27}$$

independent of σ_s. It should be noted that if the condition $k\sigma_s < 1$ is breached, then the Gaussian decay in p present in (22) becomes the dominant feature and instead a limiting plateau level

$$\Delta s = \sigma_s$$

occurs, see figure 4. Note that in this case the plateau extends all the way to $z = 0$ and the linear regime of case (i) is not seen.

Finally, regime (iii) applies once evolution of the phase space takes effect in the propagating region $|p|^2 \leqslant 1$. Assuming the quasihomogeneous case $\sigma_x \gg l$, we obtain for a given midpoint x that the finite size of the source reduces the support in p of the Wigner function and (26) is replaced by

$$W_z(x, p) \sim \begin{cases} 1, & \dfrac{x - l/2}{\sqrt{z^2 + (x - l/2)^2}} < p < \dfrac{x + l/2}{\sqrt{z^2 + (x + l/2)^2}}, \\ 0, & \text{otherwise.} \end{cases}$$

For simplicity consider the case $x = 0$. Then the CF obtained from the inverse Fourier transform of this function is

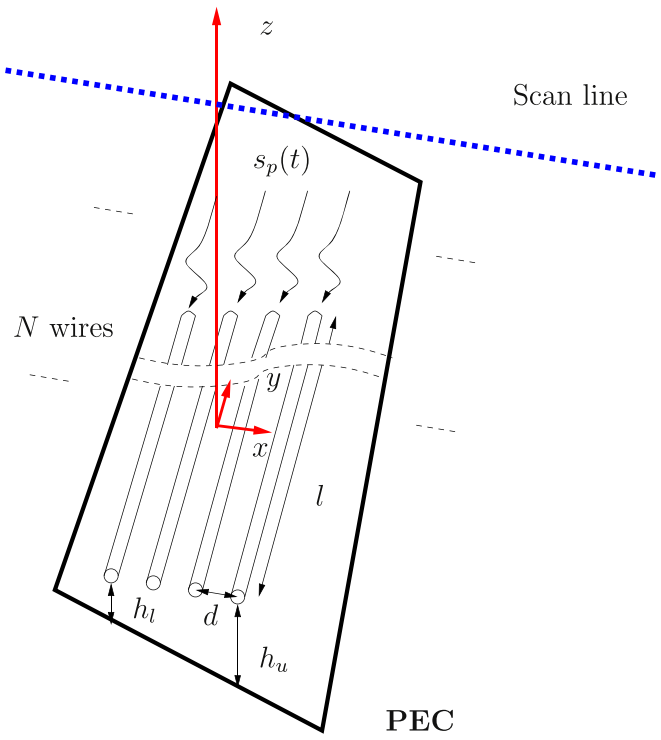

Figure 5. Set of parallel metallic wires running above an oblique perfect electric conductor (PEC) ground plane. This complex source emits radiation in the half-space $z > 0$. The full-wave TLM simulation has been carried out for the configuration with $N = 12$. (Only 4 wires are shown here for convenience). The scan line (blue dashed line) is located at $y = 0$ m at various levels of z. It is wider than the physical width of the wire array in the x direction.

$$\Gamma_z(s) \sim \frac{1}{\pi}\mathrm{sinc}\left(\frac{ks}{\sqrt{1+(2z/l)^2}}\right)$$

and the correlation length defined by (23) takes the form

$$\Delta s \approx 0.2617\lambda\sqrt{1+(2z/l)^2}\,, \tag{28}$$

generalizing (27). Going now to the farfield $kz > kz_c$, we find

$$\Delta s \approx 0.2617 \times \frac{2z\lambda}{l},$$

(where the numerical prefactor is particular to the convention (23)). Alternatively, if $\sigma_x \ll l$, then the screen length becomes unimportant and σ_x provides the length scale appropriate to the source intensity. An analogous calculation then allows us instead to recover the basic form

$$\Delta s \approx \frac{1}{2\pi} \times \frac{z\lambda}{\sigma_x}$$

of the VCZT for $z \gg \sigma_x$.

4.3. Application to a complex source

The field at the source at $z = 0$ is often produced by a complex process such as tracks on a PCB or integrated circuits in electronic devices; the radiation produced in the source region then propagates into free space. We model such a complex source here by a set of N metallic wires driven by random time-domain voltages, as illustrated in figure 5; a realization of the voltage $s_p(t)$ driving a pin of the bundle is reported in figure 6 along with its spectrum $S_p(f)$. The voltage has been generated with a uniform distribution between -0.5 and 0.5 V with a time step of 500 ps. This represents a typical problem in EMC where one tries to obtain statistical information about an erratic signal.

The presence of a perfect electric conductor (PEC) along an oblique plane makes the source radiate only into the half-space $z > 0$: this mimics a configuration that is widely used in the design of PCBs. We use $N = 12$ wires very close to each other and to the metallic plane in terms of wavelength. The wires are positioned in the plane $z = 0$ m, along the y direction, at $x = -0.33, -0.27, -0.21, -0.15, -0.09, -0.03, +0.03, +0.09, +0.15, +0.21, +0.27, +0.33$ m with respect to the centre at $x = 0$ m. In figure 5, only 4 wires at $x = -0.09$ m, -0.03 m,

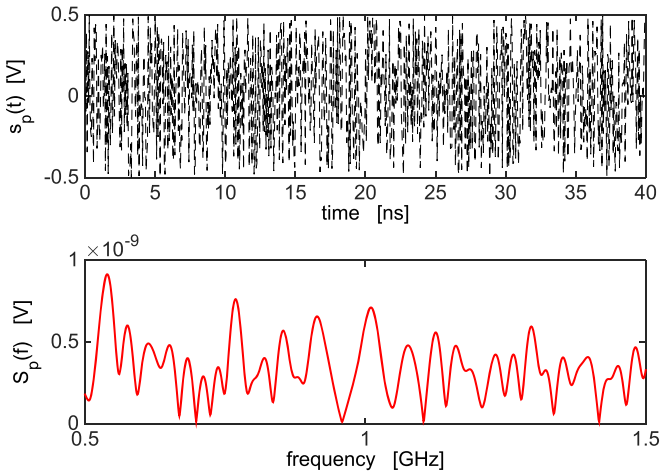

Figure 6. Time- and frequency-domain behavior of the signal driving a pin of the bundle.

+0.03 m, +0.09 m are reported for convenience. The heights h_l and h_u are referred to the wires at $x = -0.09$ m, and +0.09 m, respectively. Finally, the same *statistical* signal, i.e., fluctuating voltage varying from wire to wire but having the same statistical behaviour, is applied to all the 12 wires. Therefore, it is reasonable to think of this circuit as a collection of random sources of partially coherent radiation.

The exact fields emitted from such a complex structure are computed through an in-house transmission line matrix (TLM) code [42]. This is a time domain method for modelling 3D EM field interactions with complex structures that may include a variety of materials. The technique is based on the equivalence between electric and magnetic fields and the voltages and currents on a network of transmission lines. After discretizing space, the fields in individual cells are modelled by transmission lines incident from each cell-face and intersecting at the cell centre forming a junction. Each of these orthogonal transmission lines allows for the propagation of EM waves. The waves are characterized by voltage and current and their associated electric and magnetic fields. In order to obtain the desired CFs, we sample the numerically obtained fields in a plane above the tracks at different times in order to create a suitable ensemble of uncorrelated circuit realizations. The field recorded at the scan line $y = 0$ in figure 5 is used as a basis for calculating field-field CFs and their Wigner functions both in the near- and far-field.

Figures 7 (a) and (b) show the comparison between the WDF as computed through the full-wave (TLM) simulations, and the WDF obtained by the FP approximation (12) in the far-field at $z = 2.3\lambda$. In the TLM calculation, the full time-dependent field is propagated out from the source, while in the FP approximation, the WDF obtained from the signal at the source (as shown in figure 6, see also figure 8 (a)) is propagated according to (12). Note, that the range along the scan line $y = 0$ over which the WDF and the CF are calculated is much larger (from −3 to 3 m) than the physical width of the wire array (12×0.06 m $= 0.72$ m), see figure 7. There is good agreement between the behavior predicted from full-wave simulations and the FP approximation, even though the source exhibits strong inhomogeneities. Interestingly, figure 7 shows the same Wigner distribution shearing as in figure 2 following the geometrical interpretation (13) of the correlation propagation. It is worth stressing that such a Wigner function challenges the FP approximation (12), whose underlying assumption is quasi-homogeneity. Note that we can always also switch to the exact transport rule (8), which is computationally more expensive than the FP approximation, but still orders of magnitudes faster than a full TLM calculation. Propagated CFs as shown in figure 7 (lower plots (c) and (d)) are finally obtained by applying the inverse Fourier transform (9).

Note that we also find a pronounced broad side radiation around $p \approx \pm 1$ (corresponding to $\alpha \approx \pm\pi/2$), and a strong asymmetry of the Wigner distribution due to the oblique metallic reflector. Those features can be captured by inspection of the WDF representation in phase-space, while they are less apparent in the propagated CF shown in figures 7(c) and (d).

The source distribution $W_0(x, p)$ as obtained from the radiated signal in figure 6, is shown in figure 8(a). Note that the region with $|p|^2 > 1$ corresponds to evanescent contributions. In figures 8 (b)–(d), a comparison between WDFs as computed through the full-wave (TLM) simulations and those obtained using the WDF propagator incorporating evanescent contributions are shown along the line $x = 0$. In particular, we have used the FP approximation in equation (12) for $|p|^2 \leqslant 1$, and the evanescent approximation in equation (16) for $|p|^2 > 1$. We find that propagation beyond $z = 0.1\ \lambda$ results predominantly in an exponential reduction of the

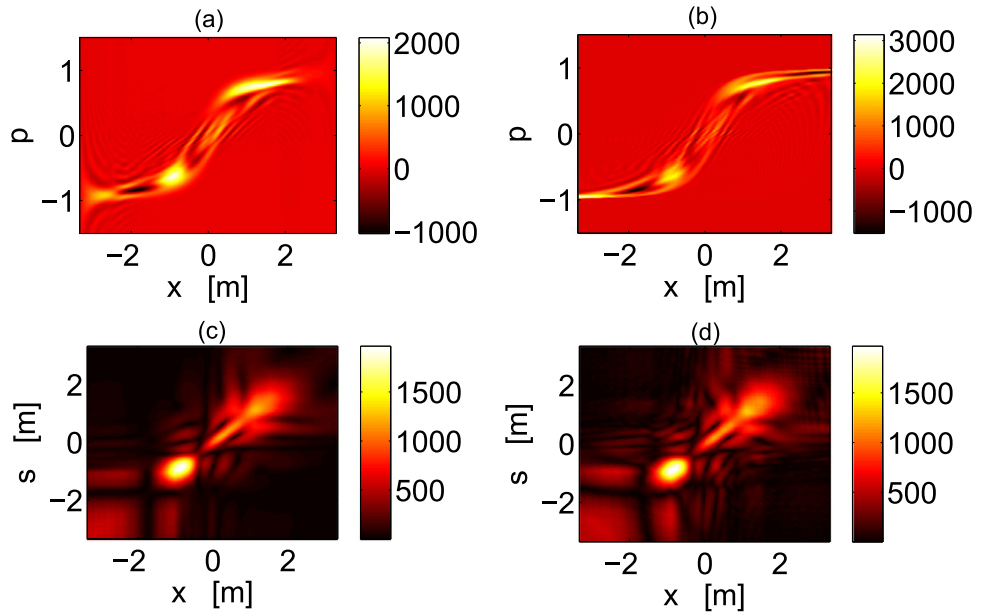

Figure 7. Far-field WDF $\Re\{W_z\}$ -(a) and (b) - and correlation functions $\| \Gamma_z \|$- (c) and (d) - at $z = 2.3\ \lambda$: comparison between TLM computation (left column) and Frobenius–Perron analytical approximation (12) (right column). The propagated correlation has been calculated through (9).

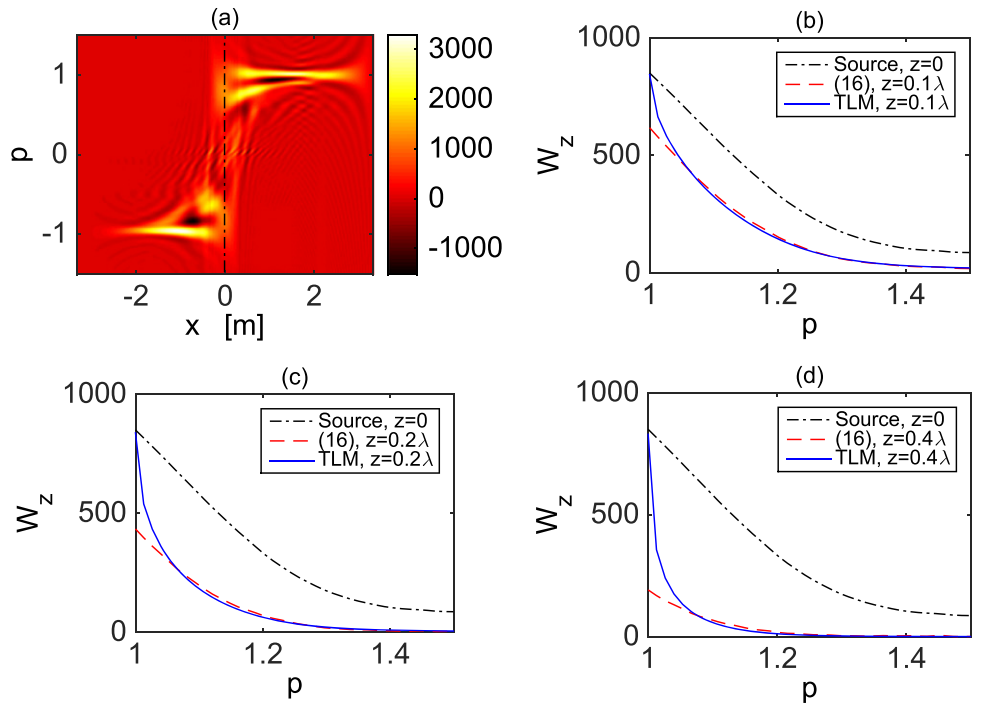

Figure 8. (a) Source distribution; near-field $\Re\{W_z\}$ WDF: comparison between TLM computation and evanescent-wave approximation (16) for (b) $z = 0.1\lambda$; (c) $z = 0.2\lambda$ and (d) $z = 0.4\lambda$ along $x = 0$. The range of p at $x = 0$ is restricted between 1 and 1.5 in (b)–(d) in order to emphasize the behavior of evanescent waves in phase-space.

WDF in the region $|p|^2 > 1$. In the far-field, the radiation energy is restricted to the phase-space region $|p| \leqslant 1$, as can be seen in the WDF in figures 7(a) and (b). The results in figures 8(b)–(d) are restricted to the momentum range $1 < p < 1.5$ in order to emphasize the behaviour of the evanescent phase-space density with increasing z, thus validating equation (16).

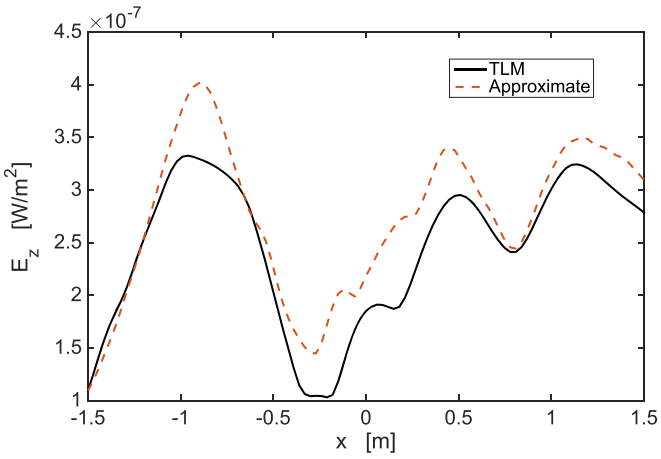

Figure 9. TLM versus approximate energy density of the field radiated far from the source.

A comparison of (TLM) simulated and (FP) approximate far-field propagated energy

$$E_z = \frac{1}{2}\,\epsilon_0\,|\psi(x)|^2 = \frac{1}{2}\,\epsilon_0 \int W_z(x,\,p)\,\mathrm{d}p, \tag{29}$$

is shown in figure 9. We see that the two numerical methods show qualitatively the same features, however, there are quantitative differences. We think that these deviations are due to a difference in the numerical treatment of the boundary conditions at $x = \pm 3$ m. While the FP approach has no difficulties in treating these boundaries as completely open, the TLM method needs to model this with absorbing boundary conditions. These conditions tend to be still slightly reflective, as is evident from the source distribution in figure 8(a) around $x = \pm 3\ m$, $p = \pm 1$. In other words, the effect of truncating the simulation domain results in a small reflection of the signal at the boundaries. Reflections interfere with each other creating a non-trivial source of discrepancy. Other sources of discrepancy may be the approximated FP propagation rule sampled for one EM field component only and along a single line. The evaluation of the WDF of actual circuits can be done for the full EM field by using the approach described here component by component.

5. Reflection of partially correlated sources

Having developed a framework for the propagation of CFs in free space, we are now interested in tackling the case of reflection from planar boundaries. In particular we would like to test the FP approximation in the presence of interference taking into account higher order corrections such as the Airy-function propagator, equation (15). It is then interesting to solve the canonical situation depicted in figure 10, where a planar reflector is located at distance $z = L$ from the source at $z = 0$.

The reflecting boundary is here for simplicity assumed to be parallel to the source plane, indefinitely extended in the $\hat{x}\hat{y}$-plane, and made of an ideal PEC. Therefore, for electric (TE) or magnetic (TM) fields perpendicular to $\hat{z}$, the Fresnel reflection coefficient reads $r(\alpha) = -1$, for all incoming angles α [43]. We again consider for simplicity only a scalar field, or a single component of the vector field, emitted from the source.

5.1. Theory

Consider a plane located at an arbitrary longitudinal coordinate $z = D$ between source and detector. The field distribution in the plane consists then of two contributions: the direct wave coming from the source, and the reflected wave bouncing off the reflector back to the source, that is,

$$\hat{\phi}(p,\,z) = \mathrm{e}^{\mathrm{i}kDT(p)}\phi(p,\,0) - \mathrm{e}^{\mathrm{i}kDT(p)+\mathrm{i}2k\Delta T(p)}\phi(p,\,0), \tag{30}$$

where $\phi(p,\,0)$ is the field at the source plane $z = 0$, $T(p)$ is defined as in (3), and $\Delta = L - D$. The momentum space CF is formed as the product of the two fields in (30) and an ensemble average is taken as in equation (1). By plugging the closed-form expression (30) into the definition of the WDF (6), we find the phase space representation

$$\mathcal{W}_D(p,\,x) = W_D(p,\,x) + W_{2L-D}(p,\,x) - \left[W_\Delta(p,\,x) + \mathrm{cc}\right], \tag{31}$$

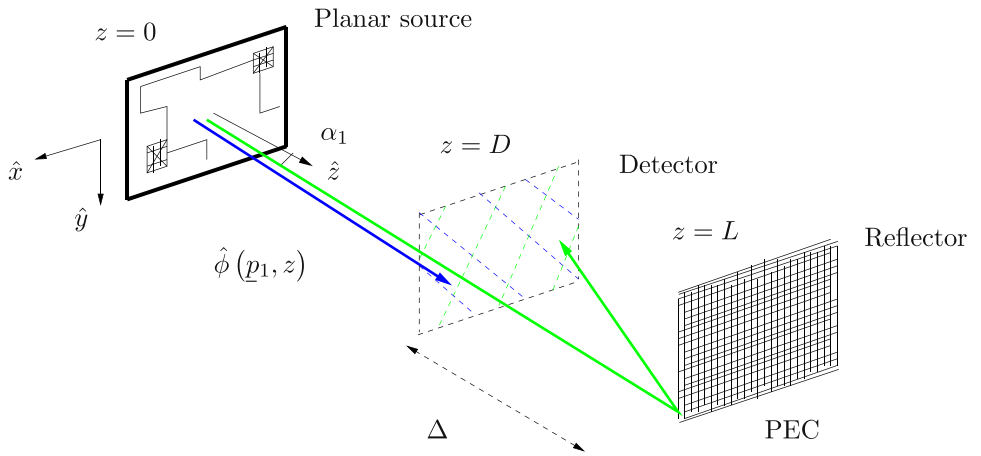

Figure 10. Arbitrary planar electromagnetic source emitting in the half-space $z > 0$, in presence of a planar metallic boundary.

where the first two terms are direct and reflected contributions respectively, coming to the detector straight from the source or through the reflector, and the last two terms express the interference between direct and reflected waves with cc standing for the complex conjugate.

Following the procedure described in the previous subsection, it can be shown that direct and reflected terms in (31) can be calculated through the free-space propagation scheme in (8) and (9), with $z = D$ and $z = 2\,L - D$ respectively, while the interference terms lead to

$$W_\Delta(p,\, x) = \int\int \mathcal{G}_\Delta(x,\, x';\, p,\, p')\, W_0(x',\, p')\, \mathrm{d}x'\mathrm{d}p', \tag{32}$$

with a modified Green integral operator

$$\mathcal{G}_\Delta(x,\, x';\, p,\, p') = \delta(p - p')\left(\frac{k}{2\pi}\right)^d \times \int \mathrm{e}^{\mathrm{i}k(x-x')q + \mathrm{i}kD\left(T\left(p+\frac{q}{2}\right) - T^*\left(p-\frac{q}{2}\right)\right) - \mathrm{i}2k\Delta T^*\left(p-\frac{q}{2}\right)}\, \mathrm{d}q. \tag{33}$$

For the class of statistically quasi-homogeneous sources, we may again expand the exponent in (33) in a Taylor series in q, and retain only terms up to first order. This results in a FP approximation of the interference terms, leading to a phase-factor of the optical length Δ besides the Dirac's delta in (11). Adopting the same linear approximation for each term in (31) gives the updated WDF

$$\mathcal{W}_D(x,\, p) \approx W_0\left(x - \frac{Dp}{T(p)},\, p\right) + W_0\left(x - \frac{(2\,L - D)p}{T(p)},\, p\right) - 2\cos\left(2k\Delta T(p)\right) W_0\left(x - \frac{Lp}{T(p)},\, p\right). \tag{34}$$

Similar expressions have been found in quantum mechanics [44] and optics [8] for two overlapping wave-functions.

Again, the propagated CF can be obtained by the inverse Fourier transform (9) of (31) or (34), the latter being closely related to the free-space VCZT.

5.2. Numerical results

We chose again an initial correlation density distributed according to the Gaussian Schell model, equation (17), with corresponding source WDF shown in figure 1. We work as usual at a frequency of operation of 1 GHz corresponding to $\lambda = 0.3$ m and choose $\sigma_x = 1.0$ m, $\sigma_s = 0.1$ m.

We further suppose a metallic mirror at $L = 1.8$ m (6λ). The propagation of the intensity from the source to the mirror can be found by evolving the source WDF with the exact rule composed of equations (8) and (9) and those for the interference terms, equations (31)–(33), and then inverse Fourier transforming the propagated WDF according to equation (9). The coherent energy $I_z(x)$ reaching the scan plane at $z = D$ is given by equation (10), that is, by considering the CF at $s = 0$.

Figure 11 shows the behavior of the intensity $I_z(x = 0)$ near the mirror, from $D = 1.0$ m to $D = 1.8$ m. The solid black line is computed through the full Green's integral operators (31) and (33), while the dashed red

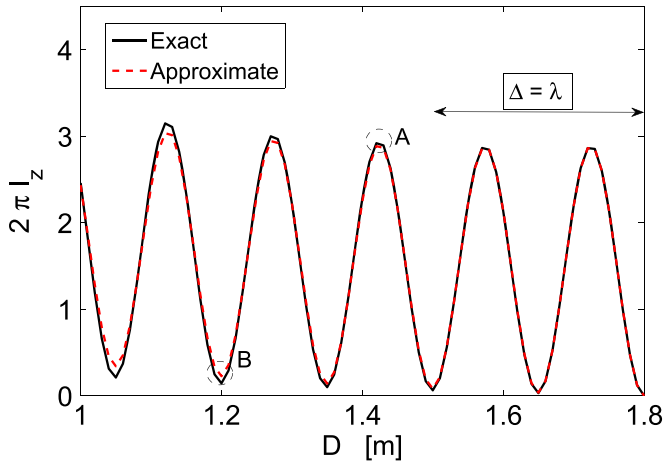

Figure 11. Interference pattern formed by the intensity $I_z(x=0)$ along the longitudinal direction as the scan plane approaches the reflector. Exact (black solid line) versus approximate (red dashed line) computations are compared.

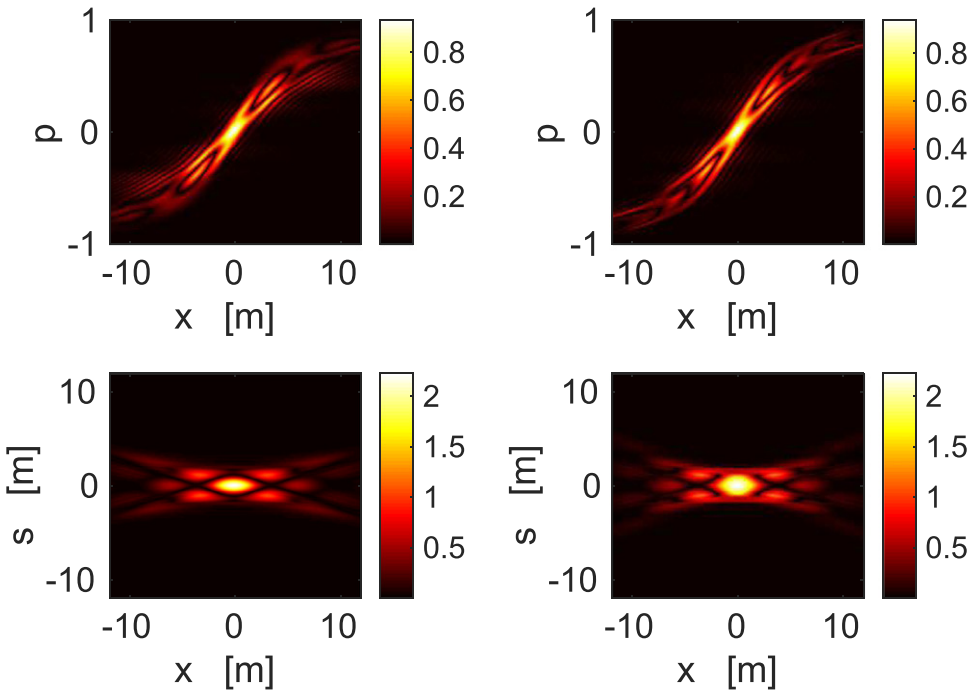

Figure 12. Magnitude of the WDF of a 1D Gaussian Schell source: exact (left plots) versus approximate (right plots) computation at $\Delta = 1.25\lambda$ (position A in figure 11). Related correlation functions are reported in the lower plots.

line is obtained by the FP approximation (34). The oscillatory behaviour in (34) is due to the interference terms in the WDF.

In figures 12 and 13, we show the magnitude of the WDF and the associated CFs at a distance $\Delta = 1.25\lambda$ (position A in figure 11) and at a distance $\Delta = 2\lambda$ (position B in figure 11) from the mirror, respectively. While good agreement between the exact and the approximate propagation using the FP approximation is achieved at position A, a maximum in the CF, the same is not true at position B. Here the intensity is suppressed due to destructive interference and the magnitude of the CF is itself only of order $O(1/k)$. To obtain the good agreement shown in figure 13, we need to take into account higher order corrections in the WDF propagator such as using the Airy function integral kernel, equation (15). The improvement when going from the leading order FP to the Airy function approximation is shown in figures 13(b) and (c), which need to be compared with the exact WF figure 13 (a); the corresponding propagated CF is displayed in figure 13(d). Only after going beyond the FP approximation in this way are we able to reconstruct the fine structure of the WDF. This finding is not surprising, but remarkable nevertheless; computing WDFs in a multi-scattering environment will encounter

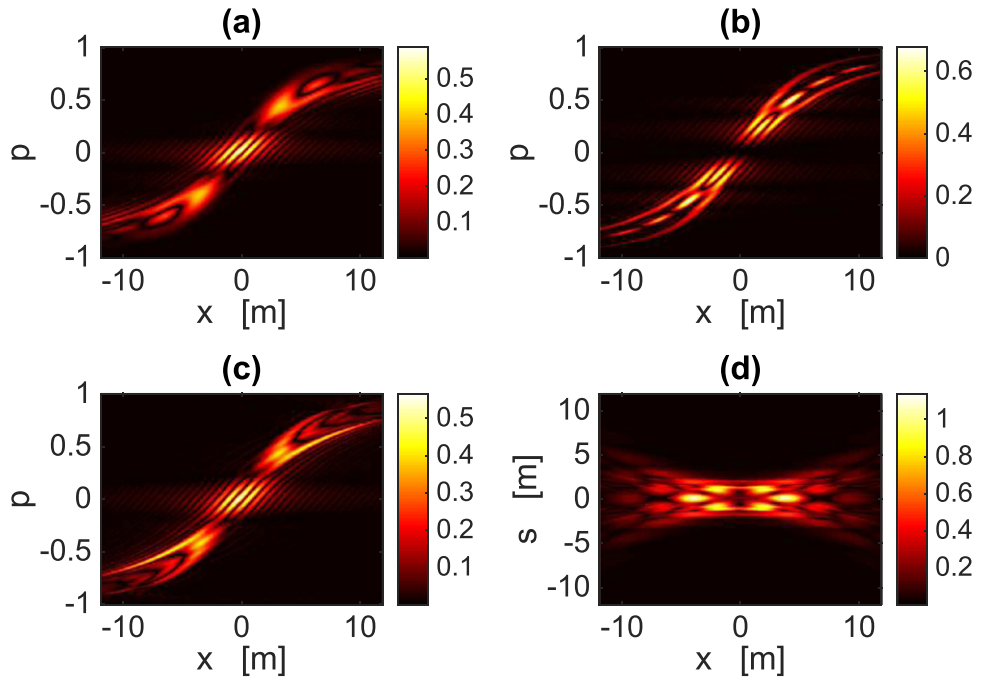

Figure 13. Magnitude of the WDF of a 1D Gaussian Schell source: exact (a) versus approximate using only FP approximation (b) and using the Airy approximation (c) at $\Delta = 2\lambda$ (position B in figure 11). The correlation function corresponding to (c) is reported in (d).

exactly these problems and we have shown that the Airy-function approximation — still faster than a full WDF propagation — can handle interference corrections successfully. We note that these corrections have been reported also in the 'diffusive' Green function presented in [19].

6. Conclusion

An exact propagator has been derived for field-field CFs of complex sources. It has been applied to a problem mimicking EM radiation from a complex source; extending this to other wave problems such as in vibro-acoustics or quantum mechanics is straightforward. The phase-space representation based on the Wigner function provides a useful means of physically interpreting the propagated data. It also serves as a very efficient computational technique both for an exact propagation of CFs and in terms of a ray approximation leading to the FP operator. This provides a good description of the propagated data even when applied to source data that are relatively far from homogeneity. Where necessary, more heterogeneous sources can be accounted for by higher-order approximations leading to an Airy propagator. This propagator proved important in the case of a planar random source emitting in presence of a planar reflector, for which we are able to reconstruct the fine structure of the phase space in presence of interference. Evanescent decay into the near field can also be accounted for using simple propagation rules. These rules have been used to investigate the effect of evanescent waves in near-field CFs. For source correlations exhibiting smaller-than-wavelength scales, we predicted a rapid initial increase of the correlation length (with distance from the source), before it saturates with the onset of the Van Cittert-Zernike behaviour at a distance of a wavelength. The approximations used have been validated through full-wave simulations using model sources and numerical sources exhibiting strong statistical inhomogeneities.

Acknowledgments

Financial supported through by the EPSRC (Grant-Ref.: EP/K019694/1) is gratefully acknowledged.

References

[1] Tanner G and Mace B 2014 *Wave Motion* **51** 547–9 (ISSN 0165-2125 innovations in Wave Modelling)
[2] Wiart J, Arnaut L and Tabbara W 2011 *Ann. Telecommun.* **66** 395–6

[3] Pinto I, Galdi V and Felsen L 2012 *Electromagnetics in a Complex World: Challenges and Perspectives* (*Springer Proc. in Physics*) (Berlin: Springer)
[4] Hill D 2009 *Electromagnetic Fields in Cavities: Deterministic and Statistical Theories* (*IEEE Press Series on Electromagnetic Wave Theory*) (New York: Wiley)
[5] Montrose M 2004 *EMC and the Printed Circuit Board: Design, Theory, and Layout Made Simple* (*IEEE Press Series on Electronics Technology*) (New York: Wiley)
[6] Hillery M, O'Connell R, Scully M and Wigner E 1984 *Phys. Rep.* **106** 121–67
[7] Dragoman D 1997 The Wigner distribution function in optics and optoelectrics *Progress in Optics XXXVII* (Amsterdam: Elsevier)
[8] Torre A 2005 *Linear Ray and Wave Optics in Phase Space: Bridging Ray and Wave Optics via the Wigner Phase-Space Picture* (Amsterdam: Elsevier)
[9] Alonso M A 2011 *Adv. Opt. Photon.* **3** 272–365
[10] Littlejohn R G and Winston R 1993 *J. Opt. Soc. Am.* A **10** 2024–37
[11] Winston R, Kim A D and Mitchell K 2006 *J. Mod. Opt.* **53** 2419–29
[12] Dittrich T and Pachón L A 2009 *Phys. Rev. Lett.* **102** 150401
[13] Berry M V 1977 *J. Phys. A: Math. Gen.* **10** 2083
[14] Hemmady S, Antonsen T M, Ott E and Anlage S M 2012 *IEEE Trans. Electromagnetic Compatibility* **54** 758–71
[15] Creagh S C and Dimon P 1997 *Phys. Rev.* E **55** 5551–63
[16] Hortikar S and Srednicki M 1998 *Phys. Rev. Lett.* **80** 1646–9
[17] Weaver R L and Lobkis O I 2001 *Phys. Rev. Lett.* **87** 134301
[18] Urbina J D and Richter K 2006 *Phys. Rev. Lett.* **97** 214101
[19] Marcuvitz N 1991 *Proc. IEEE* **79** 1350–8
[20] Cerbino R 2007 *Phys. Rev.* A **75** 053815
[21] Russer J A and Russer P 2012 Imaging of incoherent sources of radiation *Asia-Pacific Symp. on Electromagnetic Compatibility* (*APEMC*) (*Singapore, 21–24 May 2012*) pp 709–12
[22] Chappell D J, Tanner G, Löchel D and Søndergaard N 2013 *Proc. R. Soc.* A **469** 20130153
[23] Jackson J 1998 *Classical Electrodynamics* (New York: Wiley)
[24] Bucci O and Franceschetti G 1987 *IEEE Trans. Antennas Propag.* **35** 1445–55
[25] Arnaut L, Obiekezie C and Thomas D 2014 *IEEE Trans. Electromagn. Compat.* **56** 715–25
[26] Feng S, Kane C, Lee P A and Stone A D 1988 *Phys. Rev. Lett.* **61** 834–7
[27] Crisanti A, Jensen M H, Vulpiani A and Paladin G 1993 *Phys. Rev. Lett.* **70** 166–9
[28] Alonso M A 2004 *J. Opt. Soc. Am.* A **21** 2233–43
[29] Luis A 2007 *Phys. Rev.* A **76** 043827
[30] Harrington R F 1961 *Time-Harmonic Electromagnetic Fields* 1st edn (New York: McGraw-Hill)
[31] Creagh S C, Hamdin H B and Tanner G 2013 *J. Phys. A: Math. Theor.* **46** 435203
[32] Berry M V 1977 *Phil. Trans. R. Soc.* A **287** 237–71
[33] de M Rios P P and de Almeida A M O 2002 *J. Phys. A: Math. Gen.* **35** 2609
[34] Dittrich T, Viviescas C and Sandoval L 2006 *Phys. Rev. Lett.* **96** 070403
[35] Collett E and Wolf E 1980 *Opt. Commun.* **32** 27–31
[36] Ott E 2002 *Chaos in Dynamical Systems* (Cambridge: Cambridge University Press)
[37] Winston R, Sun Y and Littlejohn R G 2002 *Opt. Commun.* **207** 41–48
[38] Born M and Wolf E 1999 *Principles of Optics: Electromagnetic Theory of Propagation, Interference and Diffraction of Light* (Cambridge: Cambridge University Press)
[39] Bastiaans M 1979 *Opt. Commun.* **30** 321–6
[40] Gatti A, Magatti D and Ferri F 2008 *Phys. Rev.* A **78** 063806
[41] Carminati R and Greffet J J 1999 *Phys. Rev. Lett.* **82** 1660–3
[42] Christopoulos C 1995 *The Transmission-line Modeling Method: TLM* (*IEEE/OUP Series on Electromagnetic Wave Theory*) (Piscataway, NJ: IEEE)
[43] Tsang L and Kong J 2004 Scattering of electromagnetic waves *Scattering of Electromagnetic Waves, Advanced Topics* (New York: Wiley)
[44] Littlejohn R G 1986 *Phys. Rep.* **138** 193–291